Nano Research
2019, 12(5): 1009–1015
ISSN 1998-0124 CN 11-5974/O4
https://doi.org/10.1007/s12274-019-2331-x

Research Article

Nanoscale monitoring of mitochondria and lysosome interactions for drug screening and discovery

Qixin Chen[1,2,3], Xintian Shao[1,2,3], Zhiqi Tian[3], Yang Chen[3], Payel Mondal[4], Fei Liu[1,2], Fengshan Wang[1], Peixue Ling[1,2] (✉), Weijiang He[5] (✉), Kai Zhang[4] (✉), Zijian Guo[5], and Jiajie Diao[3] (✉)

[1] *School of Pharmaceutical Sciences, Shandong University, Jinan 250101, China*
[2] *Shandong Academy of Pharmaceutical Science, Key Laboratory of Biopharmaceuticals, Engineering Laboratory of Polysaccharide Drugs, National-Local Joint Engineering Laboratory of Polysaccharide Drugs, Jinan 250101, China*
[3] *Department of Cancer Biology, University of Cincinnati College of Medicine, Cincinnati, OH 45267, USA*
[4] *Department of Biochemistry, University of Illinois at Urbana-Champaign, Urbana, IL 61801, USA*
[5] *State Key Laboratory of Coordination Chemistry, Coordination Chemistry Institute, School of Chemistry and Chemical Engineering, Nanjing University, Nanjing 210093, China*

Received: 25 October 2018 / **Revised:** 3 February 2019 / **Accepted:** 4 February 2019

ABSTRACT

Technology advances in genomics, proteomics, and metabolomics largely expanded the pool of potential therapeutic targets. Compared with the *in vitro* setting, cell-based screening assays have been playing a key role in the processes of drug discovery and development. Besides the commonly used strategies based on colorimetric and cell viability, we reason that methods that capture the dynamic cellular events will facilitate optimal hit identification with high sensitivity and specificity. Herein, we propose a live-cell screening strategy using structured illumination microscopy (SIM) combined with an automated cell colocalization analysis software, Cellprofiler™, to screen and discover drugs for mitochondria and lysosomes interaction at a nanoscale resolution in living cells. This strategy quantitatively benchmarks the mitochondria-lysosome interactions such as mitochondria and lysosomes contact (MLC) and mitophagy. The automatic quantitative analysis also resolves fine changes of the mitochondria-lysosome interaction in response to genetic and pharmacological interventions. Super-resolution live-cell imaging on the basis of quantitative analysis opens up new avenues for drug screening and development by targeting dynamic organelle interactions at the nanoscale resolution, which could facilitate optimal hit identification and potentially shorten the cycle of drug discovery.

KEYWORDS

drug screening, mitochondria, lysosome, mitophagy, structured illumination microscopy

1 Introduction

Drug discovery and development is a cumbersome process with long turnover time and high risk [1]. It takes an average of 7.3 years and $648 million dollars to commercialize a candidate compound as a drug for clinical use [2, 3]. In recent years, technological advancements in genomics [4, 5], proteomics [6], and metabolomics [7] have largely increased the number of potential therapeutic targets. However, it remains a formidable task to identify optimal hits from the innumerable candidate compounds with high specificity and sensitivity. Commonly used cell-based drug screening techniques include 3-(4,5)-dimethylthiahiazo (-z-y1)-3,5-di-phenytetrazoliumromide staining assay (MTT) [8, 9], cell counting kit-8 assay (CCK-8) [10], enzyme-linked immunosorbent assay (ELISA) [11], and flow cytometry related assay [12, 13]. However, these tools report the cumulative level based on a large number of cells and do not resolve intracellular interactions at the single-cell level. Alternatively, fluorescent probes and optical molecular imaging techniques can be used for screening candidate drugs and evaluate their effects on individual cells [14, 15].

Dynamic organelle interactions at the nanoscale level regulate intracellular signaling outcomes and therefore represent an important target for drug screening. However, due to the diffraction of fluorescence (an infinitely small spot forms a diffuse pattern when imaged through a lens, commonly known as "Airy Disk"), even if the two objects are far apart, the "Airy Disk" may be very close [16], which inevitably limits the capacity to distinguish subcellular structure life activities at a high spatial resolution [17]. Conventionally, laser scanning confocal microscopy has been used for fast detection of high-content drug screening with high sensitivity at the cellular level [18, 19] but the far-field optical diffraction limit prevents confocal microscopy from distinguishing subcellular structures beyond 200 nm spatial resolution [20, 21]. Thus, laser scanning confocal fluorescence microscopy would not be feasible for drug screening based on dynamic organelle interactions at a nanoscale resolution [21]. Recently developed super-resolution fluorescence microscopic techniques, such as stimulated emission deletion (STED) [22, 23], structured illumination microscopy (SIM) [24], stochastic optical reconstruction microscopy (STORM) [25, 26], as well as other single-molecule super-resolution imaging techniques [27, 28], have

Address correspondence to Peixue Ling, lpxsdf@163.com; Weijiang He, heweij69@nju.edu.cn; Kai Zhang, kaizkaiz@illinois.edu; Jiajie Diao, jiajie.diao@uc.edu

provided new tools for investigating drugs for interactions between organelles at the subcellular level in living cell. However, the application of super-resolution imaging for cell-based drug screening has not been reported. SIM is a widefield microscopy technique that uses a patterned illumination (usually a stripe) to excite a sample whose stripe position and orientation can be changed multiple times and to record the emitted fluorescent signal for each of these locations, which provides a spatial resolution of up to 100 nm [21, 24]. Here, we demonstrate the use of SIM to capture dynamic organelle interaction under genetic and pharmacological interventions and point out its potential in providing new opportunities for high-content drug screening and discovery.

Mitochondria-lysosomes interactions, including fusion between mitochondria and lysosomes (mitophagy) [29] or recently discovered mitochondria-lysosome contact (MLC) [30], are important intracellular processes in eukaryotic cells. Dysfunctional mitophagy is associated with many diseases such as neurodegenerative diseases [31, 32] and cancer [33], while the dysregulated MLC is linked to Parkinson's disease [30, 31]. Although confocal fluorescence microscopy can detect mitophagy event, it is not suitable for quantitative analysis of MLC because the contact length and distance are well below 200 nm [30].

In this study, we describe a live-cell screening strategy by probing mitochondria-lysosome interaction with SIM. This strategy can resolve fine changes of mitochondria-lysosome interaction in response to genetic and pharmacological interventions at the nanoscale level in living cells. We found that genetic knockout of *ATG13*, *FIP200*, and *Penta* and pharmacological perturbation of the mTOR pathway, lysosomal pH, and ATP synthase functions cause significant changes in mitochondria-lysosome interactions. Analysis of intracellular colocalization of mitochondria and lysosomes can be automated with Cellprofiler™, a free-source imaging analysis software [34]. This work demonstrates that super-resolution imaging techniques can capture delicate intracellular organelle interactions with high sensitivity and specificity and could potentially generate improved high-throughput screening strategies with increased success rate and shorter turnover time for drug discovery and development.

2 Results and discussion

2.1 Super-resolution tracking dynamic MLC under physiological conditions

In order to observe the MLC event at the nanoscale level, we stained mitochondria with 100 nM Mito-Tracker Green (MTG) and lysosome with 200 nM Lyso-Tracker Red (LTR) in HeLa cells before imaging with SIM. As shown in Fig. 1(a), mitochondria (green color) show spherical, rod-shaped, or filamentous arrangement in an irregular manner, while lysosomes (red color) appear spherical with various sizes. In addition, a representative MLC event was captured (Fig. 1(b)), which is consistent with previous studies [21, 30].

Next, we detected the dynamic morphological change of mitochondria (Figs. 1(c) and 1(d)). Morphology of lamellar cristae was clearly visible, and dynamic progress of mitochondria separation (yellow rectangle in Fig. 1(c) and yellow arrows in Fig. 1(d)) and approach (red rectangle in Fig. 1(c) and red arrows in Fig. 1(d)) were readily captured at an approximately 130 nm lateral resolution (Fig. 1(e)), which is superior to the widefield microscopy (Fig. S1 in the Electronic Supplementary Material (ESM)). In addition, we can also capture a clear mitochondrial two-dimensional (2D) morphology (Fig. S2 in the ESM) and three-dimensional (3D) spatial distribution in whole cell (Fig. S3 in the ESM). These results indicate that SIM can resolve high-resolution morphological features previously accessed by tools such as transmission electron microscopy (TEM) or cryo-EM [10, 30]. More importantly, SIM can capture the dynamic mitochondrial processes with this high spatial resolution, which

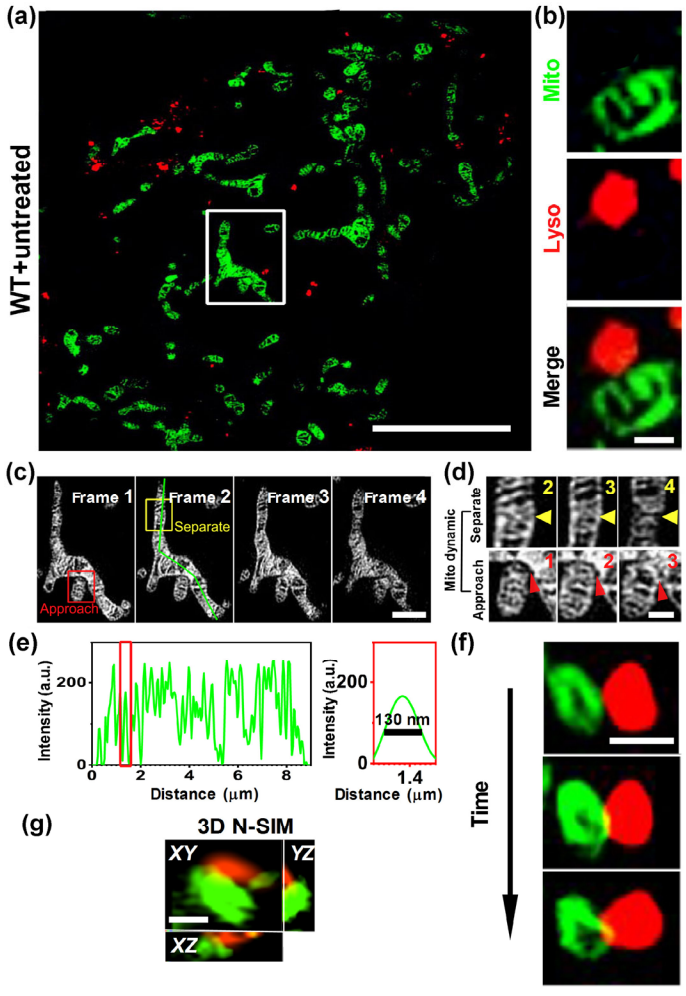

Figure 1 Subcellular morphology of mitochondria (green) and lysosomes (red) in living cells. (a) Whole cell mitochondrial and lysosomal contact under SIM. (b) A representative of mitochondria and lysosomes contact (MLC) event. (c) Nanoscale morphology of single mitochondria and characterization shown in a. (d) The dynamic processes of approach (red arrow) and separation (yellow arrow) in (c). (e) The resolution of mitochondria in c-2 (green line). (f) Dynamic processes of mitochondria and lysosomes. (g) MLC event under different sections under 3D-N SIM. Scale bar: (a) 10 μm, (b) 1 μm, (d) 0.5 μm, (f) 1 μm.

cannot be obtained by electron microscopy. As shown in Fig. 1(f), dynamic progress of MLC including mitochondrion-lysosome approach, contact, and separation was resolved using SIM. MLC events were also observed within different image projections (Fig. 1(g)). Compared to traditional tools (Fig. S5 in the ESM), SIM at 125–200 nm per frame solves the drawbacks of false positive overlap. These results suggest that SIM is an optimal tool to obtain high-resolution subcellular organelle morphological images for candidate drugs screening and discovery.

2.2 Quantitative analysis of colocalization of MLC using cell analysis software

In order to quantitatively analyze the colocalization of mitochondria and lysosomes under different conditions, we used cell profiler™, an open-source software that allows for high-throughput image analysis [34, 35]. We first captured color-merging (green-mitochondria and red-lysosome) images under SIM, and obtained grayscale images of mitochondria and lysosomes, respectively (Fig. 2(a)). The colocalization of mitochondria and lysosomes was then analyzed in cell profiler™ with the colocalization module, which measures the degree of overlap between two fluorescent channels (http://cellprofiler.org/examples/#colocalization). The resulted colocalization

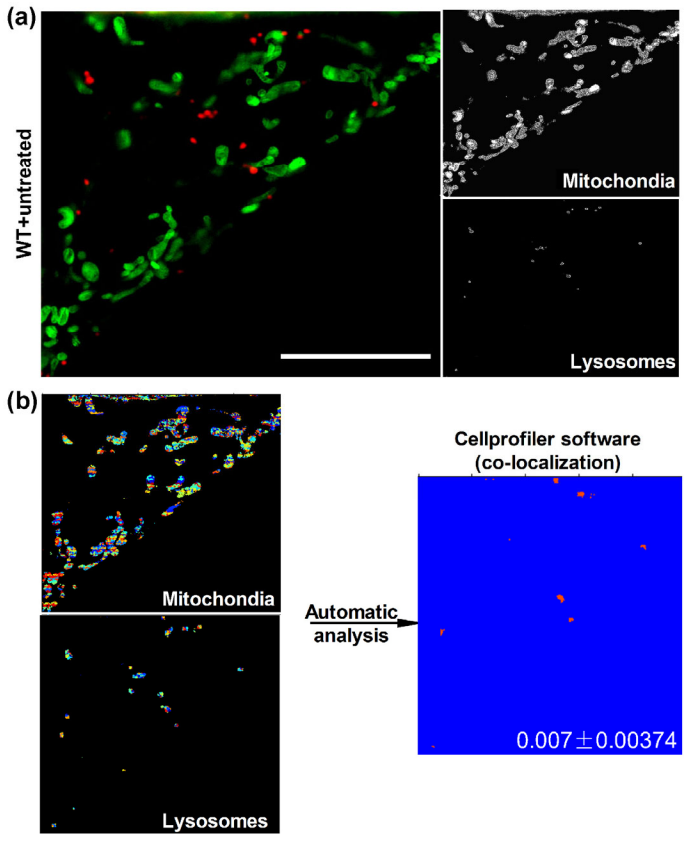

Figure 2 (a) The overlap of mitochondria and lysosomes in WT untreated cells. Scale bar: 10 μm. (b) Colocalization analysis of mitochondria and lysosomes using the Cellprofiler software.

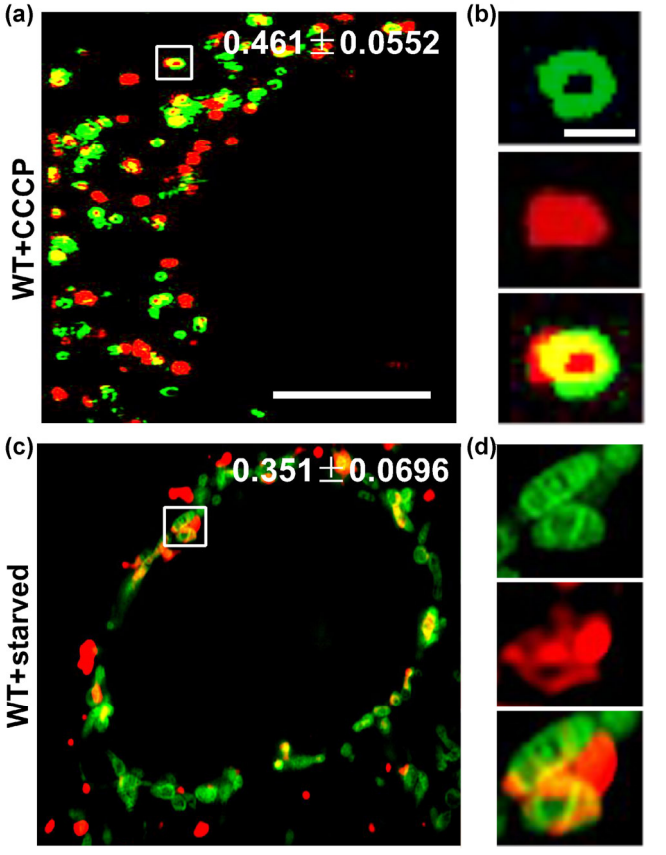

Figure 3 The mitochondria and lysosome interaction under different conditions. (a) Fusion of mitochondria and lysosomes (mitophagy) under CCCP-treatment. (b) A representative mitophagy event under CCCP-treatment. (c) The mitophagy event under starvation-treatment. (d) A representative mitophagy event under starvation stimulation. Scale bars: (a) 10 μm, (b) 1 μm.

coefficient is 0.007 ± 0.00374 (n = 6) in WT untreated cells, indicating a low mitochondria-lysosome overlap in MLC event.

2.3 Super-resolution tracking and quantitative analysis of mitophagy under pathological conditions

Autophagy includes non-selective autophagy (such as macroautophagy) and selective autophagy (such as mitophagy) [36]. Fusion between mitochondria and lysosomes is another type of mitochondrial and lysosomal interactions [21]. Under pathological conditions such as Parkinson's disease [37, 38], mitochondria are easily damaged and undergo mitophagy, or the engulfment by lysosomes, which is of great importance for normal cell growth and metabolism [39]. Thus, proteins involved in mitophagy could become perspective drug targets for the treatment of neurodegenerative diseases [40]. Such drug screening, however, requires a quantitative benchmark to differentiate mitophagy and mitochondria-lysosome fusion between normal and pathological conditions.

To induce mitophagy, we treated cells for 12 h with 10.0 μM carbonyl cyanide m-chlorophenyl hydrazone (CCCP), a commonly used mitophagy inducer [41, 42]. We then stained mitochondria and lysosomes with MTG and LTR before SIM imaging (Fig. 3(a)). After CCCP treatment, most of filamentous mitochondria seen in untreated cells (Fig. 1(a)) became spherical (Fig. 3(a)). In addition, we observed that damaged mitochondria were engulfed by lysosomes (Fig. 3(b)). We also performed additional studies to investigate mitophagy at different concentrations of CCCP treatment. We found that the number of mitophagy events was increased with CCCP concentration in individual cells (Fig. S4 in the ESM). This result indicates that the mitophagy occurs more under pathological conditions. Cellprofiler™ analysis gave a mitochondria-lysosome colocalization coefficient of 0.461 ± 0.0552 (n = 6) in stark contrast to that of untreated cell (0.007 ± 0.00374) (Fig. 2).

We then induced non-selective autophagy with an Earle's balanced salt solution (EBSS) starvation medium [43]. After EBSS starvation treatment, damaged mitochondria appeared as granules (Figs. 3(c) and 3(d)), which are similar to those in CCCP-treated cells (Figs. 3(a) and 3(b)). The mitochondria-lysosome contact increases, as evidenced by a colocalization value of 0.351 ± 0.0696 (n = 6). In addition, we readily captured damaged mitochondria engulfed by lysosomes (Fig. 3(d)).

Our results confirmed that both selective autophagy (induced by CCCP) and non-selective autophagy (induced by EBSS starvation) significantly enhance fusion of mitochondria and lysosomes. We also demonstrated that SIM enables accurate quantification of the mitochondrial and lysosomal fusion events under two different pathological conditions.

2.4 Regulation of the mitochondria-lysosome interaction by *ATG13*, *FIP200* and *Penta* genes

ATG13 and *FIP200* proteins are required for autophagy [44, 45]. To further verify the applicability SIM-based strategy in resolving mitochondria-lysosomes interaction phenotype induced by these proteins, we produced stable gene knock-out HeLa cell lines, *ATG13KO* and *FIP200KO*. WT and knock-out cells were treated with or without CCCP followed by MTG and LTR staining. In untreated *ATG13KO* and *FIP200 KO* cells, mitochondria appeared filamentous (Figs. 4(a) and 4(c)), which was similar to their WT control (Fig. 1(a)). After CCCP-treatment, damaged mitochondria appeared as granules with various sizes (Figs. 4(b) and 4(d)), which was also similar to those in CCCP-treated WT cells (Fig. 3(a)). However, colocalization coefficient analysis showed a similar value in *FIP200 KO* and *ATG13 KO* cells before (0.0780 ± 0.0249 and

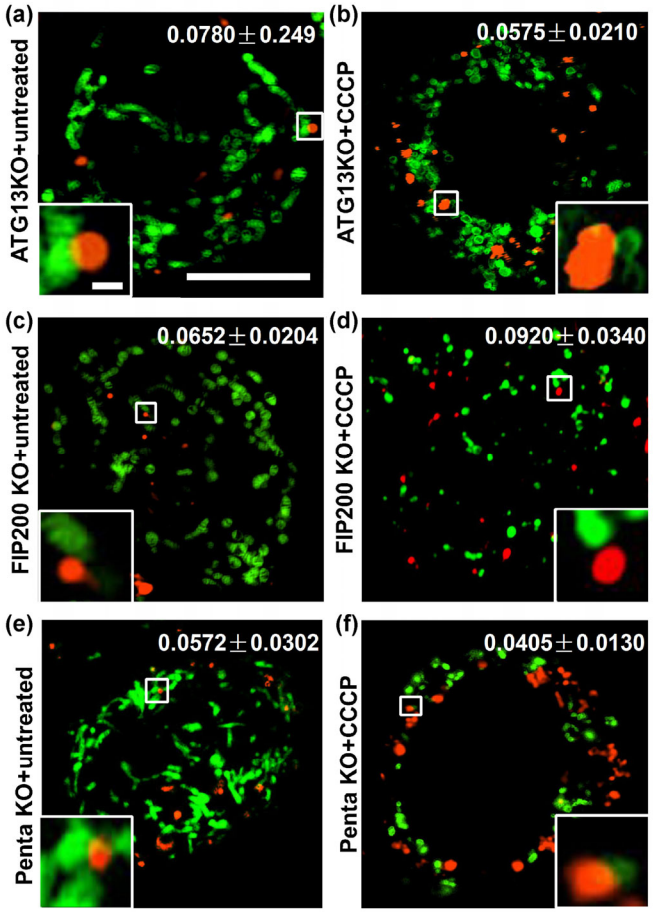

Figure 4 Interaction behavior and colocalization analysis of mitochondria and lysosomes in *ATG13KO* ((a), (b)), *FIP200KO* ((c), (d)) and *Penta KO* cells ((e), (f)) with or without CCCP. Scale bar: (a) 10 μm, inset 0.5 μm.

0.652 ± 0.0204, n = 6) and after CCCP-treatment (0.0575 ± 0.0210 and 0.092 ± 0.0340, n = 6), whereas MLC still occurred (Figs. 4(a)–4(d), inset). Together, these results demonstrate that *ATG13 KO* or *FIP200 KO* decrease the interaction between mitochondria and lysosomes in mitophagy.

Next we investigated role of different receptors (i.e., p62, NDP52, OPTN, NBR1, and TAX1BP1, denoted as *Penta*) in mitochondria-lysosome interaction and mitophagy [46, 47]. *Penta-KO* HeLa cells were treated with or without CCCP and observed under SIM. Similar to *FIP200 KO* and *ATG13 KO* cells , *Penta KO* cells showed no mitophagy changes before and after CCCP-treatment, whereas MLC still occurred (Figs. 4(e) and 4(f), inset),which is consistent with previous result [46]. These results confirm that *Penta* is needed for mitophagy. Together, it further proves that SIM combined with quantitative analysis software is an excellent tool for investigating mitochondria-lysosome interaction.

2.5 Intervention of drugs on mitochondria-lysosome interaction

Mitochondria and lysosomes interaction and fusion during mitophagy is essential for repairing damaged mitochondria [48, 49]. Recently, it has been reported that dysregulated contact sites formed by mitochondria and lysosomes are linked to Parkinson's disease [31]. We reason that proteins involved in MLC and mitophagy could serve perspective drug targets for the treatment of Parkinson's diseases. Therefore, it is reasonable to use this SIM-based strategy to investigate potential drugs for mitochondria-lysosome interaction. With this goal in mind, we tested several different target drugs in autophagy pathway for mitochondria and lysosomes interaction.

2.5.1 Intervention of rapamycin on mitochondria-lysosome interaction

Rapamycin, a specific inhibitor of mTOR protein and an autophagy inducer, binds to the intracellular receptor FKBP-12 to form a complex that directly acts on the FRB domain of mTOR to inhibit its protein activity [50, 51]. To define the effect of rapamycin on mitochondria and lysosomes interaction, we treated cells with 0.5 μM rapamycin for 12 h prior to MTG and LTR staining. After rapamycin treatment, mitochondria appeared to be granulated. In addition, lysosomal engulfment of mitochondria was clearly observed and the number of lysosomes were increased compared with untreated WT cells (Fig. 1(a)). This result indicates that rapamycin promotes fusion of mitochondria and lysosomes (autophagy), which is consistent with previous studies [52]. The colocalization coefficient under rapamycin treatment was 0.495 ± 0.0567 (n = 6) (Fig. 5(a)), which was higher than WT untreated cells (0.007 ± 0.00374, $P < 0.01$) (Fig. 2(b))(Fig. S5 in the ESM).

2.5.2 Intervention of chloroquine on mitochondria-lysosome interaction

Next, we treated the cells with an autophagy inhibitor, chloroquine that inhibits the binding of autophagosomes and lysosomes by affecting lysosomal pH [53]. After 50 μM chloroquine treatment, mitochondria appeared spherical, rod-shaped, or in filamentous arrangements, which was similar to those in untreated WT cells (Fig. 1(a)). However, the size of lysosomes increased in chloroquine-treated cells compared to that in untreated WT cells (Fig. 5(b)). In addition, no mitophagy events were observed under SIM, indicating that the binding process of autophagosomes and lysosomes was inhibited by chloroquine. Incubation of cells with both chloroquine and CCCP for 12 h caused damaged mitochondria, as shown by their spherical morphology (Fig. 5(c)). Meanwhile, MLC still occurred while no mitophagy event was observed. Addition of CCCP to chloroquine resulted in a colocalization coefficient of 0.0137 ± 0.00760 (n = 6), which was not significantly different from that under chloroquine treatment alone (0.00967 ± 0.00790, n = 6, $P > 0.05$) (Fig. S5 in the ESM).

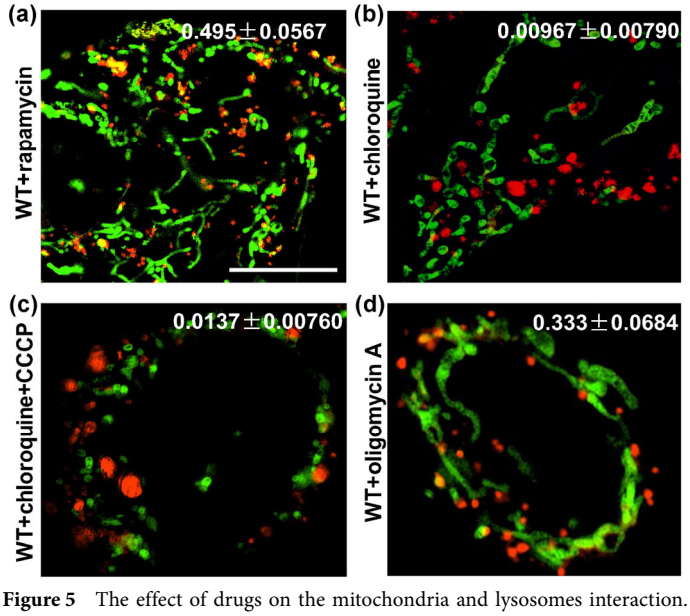

Figure 5 The effect of drugs on the mitochondria and lysosomes interaction. (a) The mitophagy event under rapamycin-treatment. (b) The mitochondria and lysosomes interaction under chloroquine-treatment. (c) The mitochondria and lysosomes interaction under chloroquine and CCCP-treatment. (d) The mitochondria and lysosomes interaction under oligomycin A-treatment. Scale bar: (a) 10 μm.

2.5.3 Intervention of oligomycin A on mitochondria-lysosome interaction

After we demonstrated that SIM can be used to study drugs for targeting mTOR and lysosomal pH, we finally determine how oligomycin A, an ATP synthase inhibitor, affects mitochondria and lysosomes interaction. By blocking ATP synthesis, oligomycin A exerts anti-tumor activity [54]. Cells were incubated with 1 μM oligomycin A for 12 h before MTG and LTR staining. Oligomycin A treatment increased the colocalization coefficient of WT cells from 0.007 ± 0.00374 (n = 6) (Fig. 2(b)) to 0.333 ± 0.0684 (n = 6) (Fig. 5(d)).

Although confocal microscopy can be used to locate mitochondria and lysosomes at the subcellular level, compared to SIM, its spatial resolution is not enough for quantitative investigation of the detailed mitochondria-lysosome interaction [55]. To compare the performance of confocal microscopy and SIM in resolving MLC and mitophagy events, we treated cells with oligomycin A and calculated the colocalization coefficient under each imaging modality (Fig. S6 in the ESM). As expected, confocal images show a high overlap of mitochondria and lysosome and was not able to clearly capture lysosomes engulfed damaged mitochondria in oligomycin A-treated cells. In contrast, mitochondria engulfed by lysosomes can be clearly observed with SIM (Fig. 5(d)). This results indicate that SIM can significant decrease the effect of fluorescence diffraction and more accurate reflect actual mitochondria and lysosome interaction than confocal microscopy.

3 Conclusions

Compared to colorimetric experiments, live-cell imaging techniques are becoming more important tools for drug discovery and screening [56]. Although colorimetric assays (MTT/CCK-8 and ELISA) allow for initial evaluation of pharmacodynamics, these methods report a simple cumulative data (such as optical density, OD) based on a large number of cells and do not detect single-cell information and subcellular organelle interactions [11]. Benefiting from simple sample preparation, fast imaging speed, and nanometer spatial resolution, the emerging SIM imaging strategy tracks the dynamic subcellular life activities and significantly expands the capacity of pharmacodynamics evaluation in high-throughput screening (Fig. S7 in the ESM).

In this study, we propose a strategy to screen and discover drugs at nanoscale level in living cells using SIM. Compared to colorimetric tools, this strategy quantitatively resolves different mitochondria-lysosome interaction in response to genetic knockout of *ATG13, FIP200* and *Penta* or pharmacological intervention targeting the mTOR pathway, lysosomal pH, and ATP synthase functionality. In addition, our findings illustrate a novel perspective of using SIM for more accurate reveal of biological activities and therapeutic effects of drugs for mitophagy and MLC events in living cells.

Cell profiler™ has been used as an analysis software in artificial intelligence for high-throughput screening [57]. Herein, we have combined artificial intelligence with super-resolution imaging to investigate living cells at the subcellular level. We have used this automated analysis software, cell profiler™, to compare colocalization of different genes and drugs for mitochondria and lysosomes interaction. Analysis with automated cell profiler™ software allowed us to process a large number of images and determine the colocalization coefficient of mitophagy and MLC rapidly. In addition, we expect to develop automated analysis software that can be loaded on the SIM platform for real-time monitoring (Fig. S8 in the ESM). Taken, together, this strategy can specifically benefit high-throughput screening of drugs as an evaluation index of pharmacodynamics in higher success rate in shorter time.

4 Experimental

4.1 Materials

Mito-Tracker Green (#M7514, MTG) and Lyso-Tracker Red (#L12492, LTR) were obtained from Invitrogen (Eugene, Oregon, USA). Carbonyl cyanide 3-chlorophenylhydrazone (#045200, CCCP), rapamycin (#12921), chloroquine diphosphate(#410950), oligomycin A (#41105) were obtained from Thermo Fisher scientific (Grand Island, NY, USA). Penicillin-streptomycin (#15140163, 10,000 units/mL), Fetal bovine serum (#26140079, FBS), Dulbecco's modified Eagle's medium (#11965118, DMEM) and other cell culture reagents were obtained from Gibco BRL (Grand Island, NY, USA).

4.2 Cell culture

HeLa cells were gifted from Dr. Carolyn M. Price lab (University of Cincinnati). *Penta* knockout HeLa cells were gifted from Dr. Richard J. Youle lab (National Institutes of Health). *ATG13* and *FIP200* knockout HeLa cells were gifted from Dr. Jun-Lin Guan lab (University of Cincinnati). Cells were cultured in Dulbecco's modified Eagle medium supplemented with 10% FBS, penicillin (100 units/mL), and streptomycin (100 μg/mL) in a 5% CO_2 humidified incubator at 37 °C.

4.3 Cell treatment and staining

A total of 2×10^5 cells were seeded on a glass bottom microwell dish and incubated with 2 mL of DMEM medium supplemented with 10% FBS for 24 h, followed by 10 μM CCCP ,0.5 μM rapamycin, 50 μM chloroquine or 1 μM oligomycin A for 12h. After treatment, the cells were washed 3 times with pre-warmed free DMEM medium, stained with 100 nM MTG for 30 min, co-incubated with 200 nM LTR at 37 °C for another 30 min, and washed with free DMEM for 3 times. Finally, cells were cultured in phenol-free medium (#1894117, Gibco, Grand Island, NY, USA) and observed under a confocal laser scanning microscopy or Nikon-SIM super-resolution microscope.

4.4 Confocal laser scanning microscopy

The images were obtained using a LSM-710 confocal laser scanning microscope (Carl Zeiss, Inc.) equipped with a 63×/1.49 numerical aperture oil-immersion objective lens and were analyzed with ZEN 2012 (Carl Zeiss, Inc.) and ImageJ software (National Institutes of Health).

4.5 Nikon-SIM super-resolution microscope imaging

Super-resolution images were acquired on a commercial Nikon-SIM Microscope (Tokyo, Japan). Images were captured with an electron-multiplying charge coupled device (EMCCD) camera iXon 897 (Andor, USA). To reduce photobleaching during SIM image acquisition, laser power was reduced to < 20% with a minimum exposure time of 200 ms for each image. Images were obtained at 512 × 512 using Z-stacks with a step size of 0.125 μm. All fluorescence images were analyzed and the background subtracted with ImageJ software (https://imagej.nih.gov/ij/) or Cell profiler software (http://cellprofiler.org/).

4.6 Co-localization Pearson correlation coefficient analysis using Cell profiler software

Co-localization Pearson correlation coefficient (the degree of overlap between two fluorescent channels, pixel-based) was quantified using the colocalization analysis plugin for Cell profiler. CellProfiler computes the linear correlation between the two channels and the slope of the line $y = ax + b$, where y and x are the two image intensities, indicating the overall relative intensity of the two images. The correlation coefficient is the normalized covariance, which is

equivalent to Pearson's correlation. Correlation ranges from −1 (complete inverse correlation) to +1 (complete correlation). Thus, larger correlation coefficients indicate stronger co-localization between two images. The calculation steps include (1) loading each channel (mitochondria-green, lysosomes-red) as a separate image, (2) correcting Illumination-Calculate, (3) correcting Illumination-Apply, and (4) measuring the extent of correlation. For more information, please refer to https://cellprofiler.org/examples/#colocalization.

Acknowledgements

This research was supported by the National Basic Research Program of China (No. 2015CB856300), Natural Science Foundation of Shandong Province (Nos. ZR2017PH072, ZR2017BH051, and ZR2015QL007), and Key Research and Development Plan of Shandong Province (No. 2018GSF121033). K. Z. was supported by the University of Illinois at Urbana-Champaign. The Light Microscopy Imaging Center (LMIC) is supported in part with funds from Indiana University Office of the Vice Provost for Research. The 3D-SIM microscope was provided by NIH grant NIH1S10OD024988-01.

Electronic Supplementary Material: Supplementary material (interaction behavior and colocalization analysis of mitochondria and lysosomes in oligomycin A-treated WT cell under a confocal microscopy, comparison of cellular drug screening tools in terms of sample preparation, processing, detection/imaging, and analysis) is available in the online version of this article at https://doi.org/10.1007/s12274-019-2331-x.

References

[1] Bialer, M.; White, H. S. Key factors in the discovery and development of new antiepileptic drugs. *Nat. Rev. Drug Discov.* **2010**, *9*, 68–82.

[2] Chen, Q. X.; Shao, X. T.; Ling, P. X.; Liu, F.; Han, G. Y.; Wang, F. S. Recent advances in polysaccharides for osteoarthritis therapy. *Eur. J. Med. Chem.* **2017**, *139*, 926–935.

[3] Prasad, V.; Mailankody, S. Research and development spending to bring a single cancer drug to market and revenues after approval. *JAMA Intern. Med.* **2017**, *177*, 1569–1575.

[4] Schulze, K.; Imbeaud, S.; Letouzé, E.; Alexandrov, L. B.; Calderaro, J.; Rebouissou, S.; Couchy, G.; Meiller, C.; Shinde, J.; Soysouvanh, F. et al. Exome sequencing of hepatocellular carcinomas identifies new mutational signatures and potential therapeutic targets. *Nat. Genet.* **2015**, *47*, 505–511.

[5] Xu, D. C.; Jin, T. J.; Zhu, H.; Chen, H. B.; Ofengeim, D.; Zou, C. Y.; Mifflin, L.; Pan, L. F.; Amin, P.; Li, W. J. et al. TBK1 suppresses RIPK1-driven apoptosis and inflammation during development and in aging. *Cell* **2018**, *174*, 1477–1491.E19.

[6] Han, M. H.; Hwang, S. I.; Roy, D. B.; Lundgren, D. H.; Price, J. V.; Ousman, S. S.; Fernald, G. H.; Gerlitz, B.; Robinson, W. H.; Baranzini, S. E. et al. Proteomic analysis of active multiple sclerosis lesions reveals therapeutic targets. *Nature* **2008**, *451*, 1076–1081.

[7] Wishart, D. S. Emerging applications of metabolomics in drug discovery and precision medicine. *Nat. Rev. Drug Discov.* **2016**, *15*, 473–484.

[8] Vega-Avila, E.; Pugsley, M. K. An overview of colorimetric assay methods used to assess survival or proliferation of mammalian cells. *Proc. West. Pharmacol. Soc.* **2011**, *54*, 10–14.

[9] Chen, Q. X.; Mei, X. F.; Han, G. Y.; Ling, P. X.; Guo, B.; Guo, Y. W.; Shao, H. R.; Wang, G.; Cui, Z.; Bai, Y. X. et al. Xanthan gum protects rabbit articular chondrocytes against sodium nitroprusside-induced apoptosis *in vitro*. *Carbohydr. Polym.* **2015**, *131*, 363–369.

[10] Chen, Q. X.; Shao, X. T.; Ling, P. X.; Liu, F.; Shao, H. R.; Ma, A. B.; Wu, J. X.; Zhang, W.; Liu, F. Y.; Han, G. Y. et al. Low molecular weight xanthan gum suppresses oxidative stress-induced apoptosis in rabbit chondrocytes. *Carbohydr. Polym.* **2017**, *169*, 255–263.

[11] Frankfurt, O. S.; Krishan, A. Enzyme-linked immunosorbent assay (ELISA) for the specific detection of apoptotic cells and its application to rapid drug screening. *J. Immunol. Methods* **2001**, *253*, 133–144.

[12] Krutzik, P. O.; Nolan, G. P. Fluorescent cell barcoding in flow cytometry allows high-throughput drug screening and signaling profiling. *Nat. Methods* **2006**, *3*, 361–368.

[13] Krutzik, P. O.; Crane, J. M.; Clutter, M. R.; Nolan, G. P. High-content single-cell drug screening with phosphospecific flow cytometry. *Nat. Chem. Biol.* **2008**, *4*, 132–142.

[14] Rudin, M.; Weissleder, R. Molecular imaging in drug discovery and development. *Nat. Rev. Drug Discov.* **2003**, *2*, 123–131.

[15] Neefjes, J.; Dantuma, N. P. Fluorescent probes for proteolysis: Tools for drug discovery. *Nat. Rev. Drug Discov.* **2004**, *3*, 58–69.

[16] Willets, K. A. Super-resolution imaging of SERS hot spots. *Chem. Soc. Rev.* **2014**, *43*, 3854–3864.

[17] Jia, S.; Vaughan, J. C.; Zhuang, X. W. Isotropic three-dimensional super-resolution imaging with a self-bending point spread function. *Nat. Photonics* **2014**, *8*, 302–306.

[18] Boutros, M.; Heigwer, F.; Laufer, C. Microscopy-based high-content screening. *Cell* **2015**, *163*, 1314–1325.

[19] Usaj, M. M.; Styles, E. B.; Verster, A. J.; Friesen, H.; Boone, C.; Andrews, B. J. High-content screening for quantitative cell biology. *Trends Cell Biol.* **2016**, *26*, 598–611.

[20] Liu, Z.; Lavis, L. D.; Betzig, E. Imaging live-cell dynamics and structure at the single-molecule level. *Mol. Cell* **2015**, *58*, 644–659.

[21] Chen, Q. X.; Jin, C. Z.; Shao, X. T.; Guan, R. L.; Tian, Z. Q.; Wang, C. R.; Liu, F.; Ling, P. X.; Guan, J. L.; Ji, L. N. et al. Super-resolution tracking of mitochondrial dynamics with an iridium(III) luminophore. *Small* **2018**, *14*, 1802166.

[22] Hanne, J.; Falk, H. J.; Görlitz, F.; Hoyer, P.; Engelhardt, J.; Sahl, S. J.; Hell, S. W. STED nanoscopy with fluorescent quantum dots. *Nat. Commun.* **2015**, *6*, 7127.

[23] Tian, X. H.; Liu, T. Y.; Fang, B.; Wang, A. D.; Zhang, M. Z.; Hussain, S.; Luo, L.; Zhang, R. L.; Zhang, Q.; Wu, J. Y. et al. Neun-specific fluorescent probe revealing neuronal nuclei protein and nuclear acids association in living neurons under STED nanoscopy. *ACS Appl. Mater. Interfaces* **2018**, *10*, 31959–31964.

[24] Huang, X. S.; Fan, J. C.; Li, L. J.; Liu, H. S.; Wu, R. L.; Wu, Y.; Wei, L. S.; Mao, H.; Lal, A.; Xi, P. et al. Fast, long-term, super-resolution imaging with Hessian structured illumination microscopy. *Nat. Biotechnol.* **2018**, *36*, 451–459.

[25] Sigal, Y. M.; Zhou, R. B.; Zhuang, X. W. Visualizing and discovering cellular structures with super-resolution microscopy. *Science* **2018**, *361*, 880–887.

[26] Huang, B.; Wang, W. Q.; Bates, M.; Zhuang, X. W. Three-dimensional super-resolution imaging by stochastic optical reconstruction microscopy. *Science* **2008**, *319*, 810–813.

[27] Ha, T.; Tinnefeld, P. Photophysics of fluorescent probes for single-molecule biophysics and super-resolution imaging. *Annu. Rev. Phys. Chem.* **2012**, *63*, 595–617.

[28] Fernández-Suárez, M.; Ting, A. Y. Fluorescent probes for super-resolution imaging in living cells. *Nat. Rev. Mol. Cell Biol.* **2008**, *9*, 929–943.

[29] Onnis, A.; Cianfanelli, V.; Cassioli, C.; Samardzic, D.; Pelicci, P. G.; Cecconi, F.; Baldari, C. T. The pro-oxidant adaptor p66SHC promotes B cell mitophagy by disrupting mitochondrial integrity and recruiting LC3-II. *Autophagy* **2018**, *14*, 2117–2138.

[30] Wong, Y. C.; Ysselstein, D.; Krainc, D. Mitochondria–lysosome contacts regulate mitochondrial fission via RAB7 GTP hydrolysis. *Nature* **2018**, *554*, 382–386.

[31] Burbulla, L. F.; Song, P. P.; Mazzulli, J. R.; Zampese, E.; Wong, Y. C.; Jeon, S.; Santos, D. P.; Blanz, J.; Obermaier, C. D.; Strojny, C. et al. Dopamine oxidation mediates mitochondrial and lysosomal dysfunction in Parkinson's disease. *Science* **2017**, *357*, 1255–1261.

[32] Tian, Z. Q.; Gong, J. H.; Crowe, M.; Lei, M.; Li, D. C.; Ji, B. H.; Diao, J. J. Biochemical studies of membrane fusion at the single-particle level. *Prog. Lipid Res.* **2019**, *73*, 92–100.

[33] Liu, K.; Lee, J.; Ou, J. H. J. Autophagy and mitophagy in hepatocarcinogenesis. *Mol. Cell. Oncol.* **2018**, *5*, e1405142.

[34] Lamprecht, M. R.; Sabatini, D. M.; Carpenter, A. E. CellProfiler™: Free, versatile software for automated biological image analysis. *Biotechniques* **2007**, *42*, 71–75.

[35] Kamentsky, L.; Jones, T. R.; Fraser, A.; Bray, M. A.; Logan, D. J.; Madden, K. L.; Ljosa, V.; Rueden, C.; Eliceiri, K. W.; Carpenter, A. E. Improved structure, function and compatibility for CellProfiler: Modular high-throughput image analysis software. *Bioinformatics* **2011**, *27*, 1179–1180.

[36] Kobayashi, S.; Liang, Q. R. Autophagy and mitophagy in diabetic cardiomyopathy. *Biochim. Biophys. Acta* **2015**, *1852*, 252–261.
[37] Ryan, B. J.; Hoek, S.; Fon, E. A.; Wade-Martins, R. Mitochondrial dysfunction and mitophagy in Parkinson's: From familial to sporadic disease. *Trends Biochem. Sci.* **2015**, *40*, 200–210.
[38] Burchell, V. S.; Nelson, D. E.; Sanchez-Martinez, A.; Delgado-Camprubi, M.; Ivatt, R. M.; Pogson, J. H.; Randle, S. J.; Wray, S.; Lewis, P. A.; Houlden, H. et al. The Parkinson's disease–linked proteins Fbxo7 and Parkin interact to mediate mitophagy. *Nat. Neurosci.* **2013**, *16*, 1257–1265.
[39] Youle, R. J.; Narendra, D. P. Mechanisms of mitophagy. *Nat. Rev. Mol. Cell Biol.* **2011**, *12*, 9–14.
[40] Li, H. Y.; Ham, A.; Ma, T. C.; Kuo, S. H.; Kanter, E.; Kim, D.; Ko, H. S.; Quan, Y.; Sardi, S. P.; Li, A. Q. Mitochondrial dysfunction and mitophagy defect triggered by heterozygous *GBA* mutations. *Autophagy* **2019**, *15*, 113–130.
[41] Williams, J. A.; Ni, H. M.; Ding, W. X. Mitochondrial dynamics, mitophagy and mitochondrial spheroids in drug-induced liver injury. In *Mitochondria in Liver Disease*. Han, D.; Kaplowitz, N., Eds.; Apple Academic Press Inc.: Florida, **2015**; pp 237.
[42] Maldonado, E. N.; Gooz, M.; DeHart, D. N.; Lemasters, J. J. VDAC opening drugs to induce mitochondrial dysfunction and cell death. *Biophys. J.* **2015**, *108*, 369a.
[43] Barutcu, S. A.; Girnius, N.; Vernia, S.; Davis, R. J. Role of the MAPK/cJun NH_2-terminal kinase signaling pathway in starvation-induced autophagy. *Autophagy* **2018**, *14*, 1586–1595.
[44] Wallot-Hieke, N.; Verma, N.; Schlütermann, D.; Berleth, N.; Deitersen, J.; Böhler, P.; Stuhldreier, F.; Wu, W. X.; Seggewiß, S.; Peter, C. et al. Systematic analysis of ATG13 domain requirements for autophagy induction. *Autophagy* **2018**, *14*, 743–763.
[45] Liu, F.; Guan, J. L. FIP200, an essential component of mammalian autophagy is indispensible for fetal hematopoiesis. *Autophagy* **2011**, *7*, 229–230.
[46] Lazarou, M.; Sliter, D. A.; Kane, L. A.; Sarraf, S. A.; Wang, C. X.; Burman, J. L.; Sideris, D. P.; Fogel, A. I.; Youle, R. J. The ubiquitin kinase PINK1 recruits autophagy receptors to induce mitophagy. *Nature* **2015**, *524*, 309–314.
[47] Li, F. X.; Xu, D. C.; Wang, Y. L.; Zhou, Z. X.; Liu, J. P.; Hu, S. C.; Gong, Y. K.; Yuan, J. Y.; Pan, L. F. Structural insights into the ubiquitin recognition by OPTN (optineurin) and its regulation by TBK1-mediated phosphorylation. *Autophagy* **2018**, *14*, 66–79.
[48] Youle, R. J.; Van Der Bliek, A. M. Mitochondrial fission, fusion, and stress. *Science* **2012**, *337*, 1062–1065.
[49] Novak, I. Mitophagy: A complex mechanism of mitochondrial removal. *Antioxid. Redox Signal.* **2012**, *17*, 794–802.
[50] Vakifahmetoglu-Norberg, H.; Xia, H. G.; Yuan, J. Y. Pharmacologic agents targeting autophagy. *J. Clin. Invest.* **2015**, *125*, 5–13.
[51] Xu, Y. Q.; Yuan, J. Y.; Lipinski, M. M. Live imaging and single-cell analysis reveal differential dynamics of autophagy and apoptosis. *Autophagy* **2013**, *9*, 1418–1430.
[52] Cristofani, R.; Marelli, M. M.; Cicardi, M. E.; Fontana, F.; Marzagalli, M.; Limonta, P.; Poletti, A.; Moretti, R. M. Dual role of autophagy on docetaxel-sensitivity in prostate cancer cells. *Cell Death Dis.* **2018**, *9*, 889.
[53] Mauthe, M.; Orhon, I.; Rocchi, C.; Zhou, X. D.; Luhr, M.; Hijlkema, K. J.; Coppes, R. P.; Engedal, N.; Mari, M.; Reggiori, F. Chloroquine inhibits autophagic flux by decreasing autophagosome-lysosome fusion. *Autophagy* **2018**, *14*, 1435–1455.
[54] Quintana-Cabrera, R.; Quirin, C.; Glytsou, C.; Corrado, M.; Urbani, A.; Pellattiero, A.; Calvo, E.; Vázquez, J.; Enríquez, J. A.; Gerle, C. et al. The cristae modulator Optic atrophy 1 requires mitochondrial ATP synthase oligomers to safeguard mitochondrial function. *Nat. Commun.* **2018**, *9*, 3399.
[55] Chen, Q. X.; Shao, X. T.; Hao, M. G.; Tian, Z. Q.; Wang, C. R.; Liu, F.; Zhang, K.; Wang, F. S.; Ling, P. X.; Guan, J. L. et al. Quantitative analysis of interactive behavior of mitochondria and lysosomes using structured illumination microscopy. 2018, *bioRxiv*: https://doi.org/10.1101/445841.
[56] Zemanová, L.; Schenk, A.; Valler, M. J.; Nienhaus, G. U.; Heilker, R. Confocal optics microscopy for biochemical and cellular high-throughput screening. *Drug Discov. Today* **2003**, *8*, 1085–1093.
[57] Simm, J.; Klambauer, G.; Arany, A.; Steijaert, M.; Wegner, J. K.; Gustin, E.; Chupakhin, V.; Chong, Y. T.; Vialard, J.; Buijnsters, P. et al. Repurposing high-throughput image assays enables biological activity prediction for drug discovery. *Cell Chem. Biol.* **2018**, *25*, 611–618.e3.